https://doi.org/10.5194/egusphere-2025-2210
Preprint. Discussion started: 17 June 2025

Measurement report: Variations and environmental impacts of atmospheric N_2O_5 concentrations in urban Beijing during the 2022 Winter Olympics

Tiantian Zhang[1], Peng Zuo[2], Yi Chen[2], Tong Liu[1], Linghan Zeng[2], Weili Lin[1,3*], Chunxiang Ye [2*]

[1]NEAC Key Laboratory of Ecology and Environment in Minority Areas, College of Life and Environmental Sciences, Minzu University of China, Beijing, 100081, China

[2]State Key Joint Laboratory for Environmental Simulation and Pollution Control, College of Environmental Sciences and Engineering, Peking University, Beijing, 100871, China

[3]Institute of National Security, Minzu University of China, Beijing, 100081, China

Correspondence to: Weili Lin (linwl@muc.edu.cn) and Chunxiang Ye (c.ye@pku.edu.cn)

https://doi.org/10.5194/egusphere-2025-2210
Preprint. Discussion started: 17 June 2025

Abstract. The chemistry of nitrate radical (NO_3) and dinitrogen pentoxide (N_2O_5) plays a pivotal role in tropospheric nighttime chemistry. Given their close linkage to precursor variations, emission reduction during the 2022 Beijing Winter Olympics likely affected NO_3 and N_2O_5 behavior. In this study, we measured N_2O_5, NO_2, O_3, etc. during and after the Olympics, and compared pollutant levels as well as the contributions of reaction pathways to the loss of NO_3 and N_2O_5. Throughout the entire observation period, NO_3 production rate averaged 0.5 ± 0.4 ppbv h^{-1}, and the N_2O_5 mixing ratio could reach up to 875 pptv within 1 min, indicating their active production. The relatively long $\tau(N_2O_5)$ at night, with an average of 11.9 ± 11.8 minutes, suggested a slow rate of N_2O_5 loss during the winter season. Despite low NO (below 3 ppbv), it dominated NO_3 loss (79.0 %). VOCs oxidation contributed 0.2 %, mainly from styrene. During the Olympics, emission reductions led to decreased NO and VOCs, which in turn reduced their reaction with NO_3. The heterogeneous uptake of N_2O_5, another NO_3 loss pathway, accounted for 20.8 % during the event and 10.6 % afterward. This uptake is crucial for NO_3 removal at night, and would be essential for winter nitrate formation in urban Beijing.

1 Introduction

Nitrate radical (NO_3) and dinitrogen pentoxide (N_2O_5) play crucial roles in the nocturnal atmospheric chemical cycle, controlling the removal and conversion of nitrogen oxides (NO_x) and volatile organic compounds (VOCs). They significantly contribute to the formation of nitrate and secondary organic aerosols during the nighttime (Crutzen, 1979; Wayne et al., 1991). NO_3 primarily originates from the reaction between NO_2 and O_3, encapsulated in the reaction scheme (R1). Given the swift thermodynamic equilibrium (R2) between NO_3 and N_2O_5, these species are frequently considered in tandem. During daytime, the rapid photolysis of NO_3 (R3) and its reaction with NO (R4) result in a short NO_3 lifetime (< 5 s). Consequently, the concentrations of NO_3 and N_2O_5 usually fall below the detection limit of analytical instruments during daylight hours.

The direct removal pathways of NO_3 include heterogeneous reactions on the surface of particulate matter and gas-phase reactions with NO (R4) and VOCs (R5), which can influence the atmospheric lifetimes of nighttime NO_x and VOCs (Ng et al., 2017; Wayne et al., 1991). NO_3 is also capable of reacting with alkenes in an addition reaction (R5) and subsequently with O_2 to form RO_2, which further generates organic nitric acid, one of the important sources of secondary organic aerosols (Fry and Sackinger, 2012; Hoyle et al., 2007; Pye et al., 2010). The removal pathways of N_2O_5 represent indirect removal pathways for NO_3 chemistry (R6), primarily involving reactions with water vapor and heterogeneous reactions on cloud droplets and particle surfaces (Brown and Stutz, 2012; Chang et al., 2011).

$$NO_2 + O_3 \rightarrow NO_3 + O_2 \quad \text{(R1)}$$

$$NO_2 + NO_3 \leftrightarrows N_2O_5 \quad \text{(R2)}$$

$$NO_3 + h\nu \rightarrow O_2 + NO \quad \text{(R3)}$$

https://doi.org/10.5194/egusphere-2025-2210
Preprint. Discussion started: 17 June 2025

$NO_3 + NO \rightarrow 2NO_2$ (R4)

$NO_3 + VOC \rightarrow$ products (R5)

$N_2O_5 + H_2O\ (l) \rightarrow 2HNO_3$ (R6)

In recent years, anthropogenic emission control measures have played a pivotal role in improving air pollution in China (Li et al., 2020; Zhang et al., 2016). Despite a declining trend in NO_x emissions in China over the past decades, the emission intensity remains relatively high (Li et al., 2024). Reactive nitrogen-containing compounds have emerged as a prominent factor in China's complex air pollution scenario (Zhu et al., 2023). With advancements in measurement techniques, several research teams have explored the core processes of reactive nitrogen species in atmospheric pollution, particularly in regions with severe atmospheric pollution such as the North China Plain, the Yangtze River Delta, and the Pearl River Delta (Li et al., 2020; Tham et al., 2016; Wang et al., 2018, 2020, 2024, 2013; Yun et al., 2018). While NO_3 reactivity is typically attenuated under low-temperature winter conditions, thereby restricting its oxidative capacity, multiple studies—including winter campaigns such as Yun et al. (2018) and Yan et al. (2023)—have demonstrated the significance of nocturnal NO_3 chemistry in cold seasons.

Recent studies have indicated that the increase in the nocturnal NO_3 production rates leads to enhanced nocturnal oxidation (Wang et al., 2023a). Under the influence of emission reduction policies, nocturnal NO_3 radicals in urban areas may experience an "explosive" increase (Wang et al., 2023b), and the contribution of nocturnal nitrogen chemistry to winter haze formation in the Beijing area has risen (Yan et al., 2023). Despite these efforts, there is still a lack of comprehensive understanding and continuous monitoring of the chemical processes of reactive nitrogen-containing compounds like NO_3 and N_2O_5.

During the 2022 Winter Olympics, a series of emission reduction measures were implemented in and around Beijing to safeguard air quality. As a result, the average $PM_{2.5}$ concentration in Beijing was 24 μg m^{-3}, a significant improvement compared to historic levels during the same period (Huang et al., 2024). Given their close linkage to precursor variations, the 2022 Beijing Winter Olympics' emission cuts likely affected NO_3 and N_2O_5 behavior. In this study, we carried out observational research during and after the Olympics to understand the nocturnal chemistry of NO_3 and N_2O_5 in urban Beijing, to unravel the balance and loss mechanisms of NO_3 and N_2O_5, and to assess the impacts of emission reduction measures on their nocturnal chemistry.

2 Methods

2.1 Site description

Measurements were conducted from 5 February to 3 March 2022. The study site was situated on the rooftop of the NO. 1 Science Building at Peking University in Beijing (39.99° N, 116.31° E, 61.6 m asl). As shown in Fig.

https://doi.org/10.5194/egusphere-2025-2210
Preprint. Discussion started: 17 June 2025

1, the location is proximal to two traffic arteries along the North Fourth Ring Road, rendering it representative of an urban site, as corroborated by previous studies (Hu et al., 2023; Wang et al., 2017b; Yao et al., 2023).

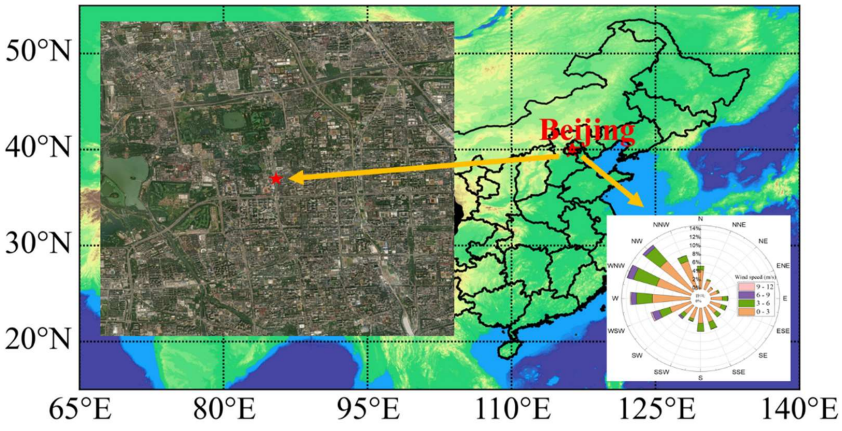

Figure 1. Measurement Site, Surroundings & Wind Rose (Winter 2022).

The sampling inlets were positioned at a height of 1.5 meters above the rooftop, approximately 20 meters above ground level. Throughout the measurement period, the prevailing wind direction was predominantly from the northwest, with an average wind speed of 2.0 ± 2.0 m s^{-1}.

2.2 Instrument setup

In this study, the ambient concentrations of NO_3 were determined utilizing an in-house-developed cavity ring-down spectroscopy (CRDS) analyzer, whereas N_2O_5 was quantified through its thermal decomposition to NO_3. A comprehensive elucidation of the measurement techniques and parameter quantification methodologies is elaborated upon in our prior research (Zhang et al., 2024). Due to a malfunction in the NO_3 measurement chamber, only the aggregate concentration of N_2O_5 + NO_3 could be ascertained. The instrument's limit of detection was established at 2.9 pptv (1σ), with an associated measurement uncertainty of ± 13.7 %. For the calibration of the observational data, a stable source of N_2O_5 and NO_3 generation was employed to quantify the losses incurred during gas path transport, encompassing both tubing and filter losses (Zhang et al., 2026). It revealed that the tubing loss amounted to 11.4 %, while the filter membrane loss was recorded at 4.5 % ± 0.5 %.

Other measured parameters include NO, NO_2, O_3, VOCs, and meteorological factors. NO and O_3 mixing ratios were measured using commercial instruments, specifically the Model 42i-Y and Model 49i from Thermo Fisher Scientific (USA). NO_2 mixing ratios were observed via a cavity-enhanced absorption spectroscopy (CEAS) (Zhou et al., 2022). VOC concentrations were determined using a gas chromatograph equipped with mass spectrometry and flame ionization detectors (Wang et al., 2014). Meteorological parameters, including wind direction, wind speed, temperature (T), and relative humidity (RH), were monitored utilizing a sensor

https://doi.org/10.5194/egusphere-2025-2210
Preprint. Discussion started: 17 June 2025

meteorological measurement system (Metone, USA). The $PM_{2.5}$ concentration data were obtained from the Beijing Municipal Ecological and Environmental Monitoring Center (bjmemc.com.cn). Detailed information about these instruments is listed in Table 1.

Table 1 Species measured in the field work

Species	Time resolution (s)	Limit of Detection/working range	Methods	Accuracy (%)	References
O_3	60	1 ppbv (parts per billion by volume)	UV photometry	± 1 %	-
NO_2	30	8 pptv	CEAS	< 6 %	(Zhou et al., 2022)
NO	60	50 pptv	chemiluminescence	± 1 %	-
N_2O_5	60	2.9 pptv	CRDS	± 18 %	(Zhang et al., 2024)
VOCs	3600	1–26 pptv	GC-MS/FID	0.8 % – 6.1 %	(Wang et al., 2014)
T	60	-50–50°C	A three-element composite thermistor	± 0.1°C	www.metone.com
RH	60	0–100 %	Thin film polymer capacitor	± 0.2 %	www.metone.com

2.3 Calculation methods

When N_2O_5 concentrations are obtained, the concentration of NO_3 can be determined by dividing the concentration of N_2O_5 by the equilibrium constant K_{eq} and the concentration of NO_2 (Osthoff et al., 2006; Wang et al., 2017c), which is specified in Eq. (1).

$$[NO_3]=\frac{[N_2O_5]}{K_{eq}[NO_2]} \quad (1)$$

Here, K_{eq} represents the temperature-dependent equilibrium constant established when NO_3 attains steady-state equilibrium with N_2O_5, and is given by $5.50\times10^{-27}\times \exp(10724/T)$, where T is the temperature in Kelvin (Wang et al., 2024).

The primary source of NO_3 and N_2O_5 is the chemical reaction of NO_2 with O_3. Consequently, the concentrations of NO_2 and O_3 are key factors influencing the production rate of NO_3 ($P(NO_3)$). This production rate is mathematically represented by Eq. (2) (Brown et al., 2011). Assuming that the formation and loss processes of NO_3 and N_2O_5 are in a state of dynamic equilibrium, the lifetime of N_2O_5, denoted as $\tau_{N_2O_5}$, can be expressed as the ratio of its concentration to the rate of NO_3 production, as determined by Eq. (3) (Brown and Stutz, 2012; Lin et al., 2022; Wang et al., 2017b).

https://doi.org/10.5194/egusphere-2025-2210
Preprint. Discussion started: 17 June 2025

$$P(NO_3) = k_{NO_2+O_3} \times [NO_2] \times [O_3] \quad (2)$$

$$\tau_{N_2O_5} = \frac{[N_2O_5]}{P(NO_3)} = \frac{[N_2O_5]}{k_{NO_2+O_3} \cdot [NO_2] \cdot [O_3]} \quad (3)$$

The primary sinks for NO_3 can be attributed to the following four mechanisms:

(a) Photolytic decomposition,

(b) Reaction with NO,

(c) Reaction with VOCs,

(d) Heterogeneous uptake by N_2O_5.

The total NO_3 reactivity (k_{NO_3}) is determined using Eq. (4) (Wang et al., 2020). The nocturnal NO_3 loss rate, denoted as $L(NO_3)$, is calculated via Eq. (5).

$$k_{NO_3} = j(NO_3) + k_{NO_3+NO} \cdot [NO] + k_{NO_3+VOCs} \cdot [VOCs] + k_{N_2O_5} \cdot K_{eq} \cdot [NO_2] \quad (4)$$

$$L(NO_3) = \sum k_i [VOC_i] \cdot [NO_3] + k_{NO_3+NO} \cdot [NO][NO_3] + k_{N_2O_5} \cdot [N_2O_5] \quad (5)$$

Here, $j(NO_3)$ denotes the photolysis rate constant for NO_3 decomposition. The rate coefficients $k_{NO_2+O_3}$ and k_{NO_3+NO} correspond to the rate coefficients for reaction Eqs. (1) and (4), respectively, as referenced in Atkinson et al. (2004). The reactivity of NO_3 with VOCs is characterized by a first order loss rate constant, calculated as the product of the reaction rate constant k_i and the VOC concentrations $[VOC_i]$.

$k_{N_2O_5}$ represents the total first-order loss rate coefficient for the heterogeneous uptake of N_2O_5 at the aerosol surface, which is governed by the uptake coefficient $\gamma(N_2O_5)$, the aerosol surface area density S_a ($\mu m^2\ cm^{-3}$), and the mean molecular speed of N_2O_5, c. $\gamma(N_2O_5)$ is influenced by the components of particulate matter and atmospheric environmental conditions (e.g., humidity and temperature) (Bertram et al., 2009; Tang et al., 2014; Yu et al., 2020).

$$k_{N_2O_5} = \frac{1}{4} c S_a \gamma(N_2O_5) \quad (6)$$

Under the steady-state assumption, $\gamma(N_2O_5)$ is determined by the slope of the linear regression between $K_{eq}[NO_2]\tau(N_2O_5)^{-1}$ and $\frac{1}{4} c S_a \gamma(N_2O_5) K_{eq}[NO_2]$, as formalized in Eq. (7) and extensively applied to field observations (Brown et al., 2016; Lin et al., 2022; Lu et al., 2022). S_a is calculated from the $PM_{2.5}$ concentration using the empirical formula presented in Eq. (8) (Zhang et al., 2022).

$$K_{eq}[NO_2]\,\tau(N_2O_5)^{-1} = \frac{1}{4} c S_a \gamma(N_2O_5)\, K_{eq}[NO_2] + k_{NO_3} \quad (7)$$

$$S_a = 60.03 \times [PM_{2.5}]^{0.62} \quad (8)$$

https://doi.org/10.5194/egusphere-2025-2210
Preprint. Discussion started: 17 June 2025

3 Results

3.1 Measurements overview

Figure 2 illustrates the time-series variations in the mixing ratios of N_2O_5 and associated trace gases, alongside meteorological parameters, captured during the 2022 Beijing Winter Olympics (BWO) at a temporal resolution of 1 minute. Valid data were systematically acquired over a 26-day span, from 5 February to 3 March. In alignment with the 2022 Beijing Winter Olympics timeline, the observation interval was bifurcated into two distinct periods: (1) the Olympic Games Period (OGP; spanning 5-20 February), and (2) the Post-Olympics Period (POP; extending from 21 February to 3 March). Comprehensive statistical metrics for each period are meticulously detailed in Table 2.

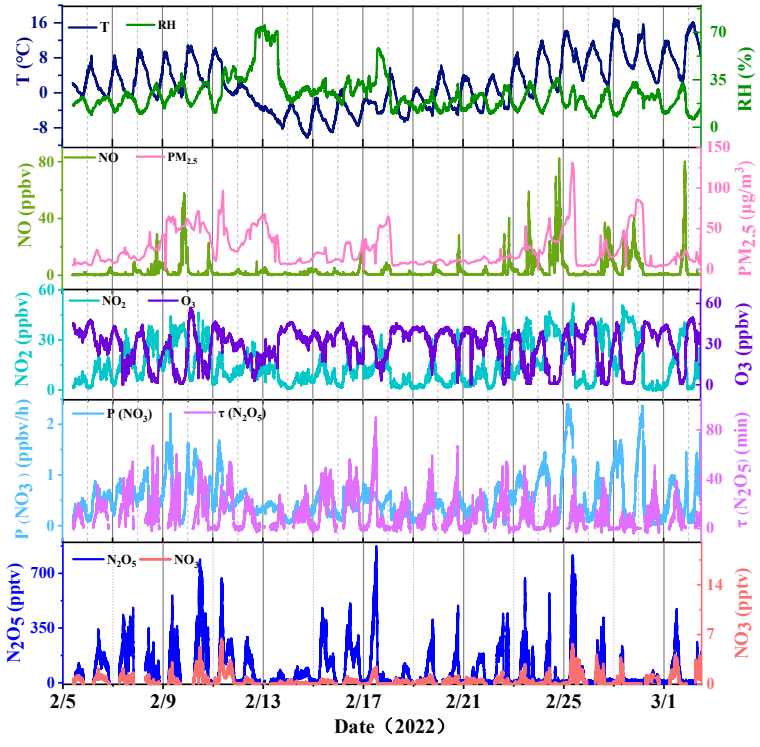

Figure 2. Time series for N_2O_5, NO_3, related trace gases, and meteorological data (T and RH) measured at Beijing from 5 February to 3 March 2022.

During the OGP, nocturnal temperatures predominantly lingered below the freezing point. A heavy snowfall event, accompanied by elevated relative humidity, occurred between February 13 and February 14, coinciding with a $PM_{2.5}$ concentration of 68 μg m^{-3}. Transitioning into the POP, ambient temperatures exhibited a marked

https://doi.org/10.5194/egusphere-2025-2210
Preprint. Discussion started: 17 June 2025

escalation from -0.4 °C to 5.6 °C, coupled with a decline in relative humidity. This period was punctuated by an episode of heightened $PM_{2.5}$ pollution, with concentrations peaking at 131 μg m^{-3}. The average $PM_{2.5}$ concentration throughout the entire observational period was 24 ± 21 μg m^{-3} and the average value of S_a was 402 ± 215 μm^2 cm^{-3}.

Table 2. Summary of observed parameters for the two periods (mean ± standard deviation).

Species	OGP		POP	
	All day	Nighttime	All day	Nighttime
O_3 (ppbv)	29.9 ± 9.5	27.4 ± 10.3	26.7 ± 10.6	19.8 ± 12.1
NO_2 (ppbv)	12.6 ± 8.2	14.5 ± 9.3	18.2 ± 12.3	20.7 ± 13.1
NO (ppbv)	1.9 ± 2.3	1.0 ± 1.2	5.7 ± 6.1	4.8 ± 6.0
N_2O_5 (pptv)	87.3 ± 71.6	137.6 ± 112.7	62.1 ± 57.7	97.8 ± 90.3
NO_3 (pptv)	0.4 ± 0.4	0.6 ± 0.6	0.3 ± 0.4	0.5 ± 0.6
$PM_{2.5}$ (μg m^{-3})	25 ± 2	26 ± 2	23 ± 3	23 ± 2
T (°C)	-0.4 ± 3.9	-1.4 ± 3.6	5.6 ± 3.9	3.5 ± 3.5
RH (%)	27.1 ± 13.3	28.6 ± 12.8	19.3 ± 4.3	20.3 ± 3.8
$P(NO_3)$ (ppbv h^{-1})	0.5 ± 0.2	0.5 ± 0.2	0.6 ± 0.4	0.5 ± 0.3
$\tau(N_2O_5)$ (min)	10.9 ± 17.0	17.0 ± 17.0	7.4 ± 4.4	11.6 ± 6.8

During the observation period, the mean concentration of O_3 was 28.6 ± 12.8 ppbv, notably lower than spring values observed in Beijing (Wang et al., 2018). Nocturnal O_3 concentrations were much higher during the OGP than those during the POP, suggesting enhanced NO_3 production rates under comparable NO_2 levels during the OGP.

The average NO_x concentration was 18.2 ± 16.6 ppbv, substantially lower than autumn values typically observed at this site (generally exceeding 30 ppbv) (Li et al., 2022; Wang et al., 2017b). During morning rush hours, the peak NO mixing ratio reached 66.6 ppbv, with an average of 3.5 ± 7.2 ppbv, a value lower than that reported for Beijing in September (6.1 ± 14.5 ppbv) (Wang et al., 2017b), and significantly below the 50.2 ± 51.4 ppbv observed by Li (Li et al., 2022).

In contrast to the POP, nocturnal NO mixing ratios decreased during the OGP, suggesting that the implementation of emission reduction policies effectively curbed primary pollutant emissions during the Winter Olympics. The subsequent increase in NO emissions facilitated its reaction with O_3 to form NO_2, leading to higher NO_2 mixing ratios during the POP compared to OGP. Elevated NO levels rapidly consumed NO_3, leading to swift decreases in both NO_3 and N_2O_5 concentrations.

During the observation period, the N_2O_5 concentrations exhibited notable fluctuations, with a mean daily value of 86.7 ± 116.5 pptv. As shown in Fig. 2, the maximum N_2O_5 mixing ratio occurred on February 18 at 00:15, reaching a value of 874.9 pptv. This value, while lower than the values previously reported for the Huairou site

https://doi.org/10.5194/egusphere-2025-2210
Preprint. Discussion started: 17 June 2025

in Beijing during the winter and the same site during the autumn (both greater than 1 ppbv) (Li et al., 2018; Wang et al., 2017b), surpassed the maximum value observed during the spring at the same site (Wang et al., 2017a). At the time of the peak N_2O_5 concentration, the measured mixing ratios of NO_2 and O_3 were 14.6 ppbv and 26.8 ppbv, respectively, with NO levels remaining relatively low at just 0.4 ppbv. The mean NO_3 mixing ratios, derived from N_2O_5 thermal equilibrium calculations, were 0.6 ± 0.7 pptv, markedly lower than observational values reported for Shanghai (16 ± 9 pptv) (Wang et al., 2013).

Table 3 presents a comparative analysis of the mixing ratios of N_2O_5 and NO_3, $P(NO_3)$, and $\tau(N_2O_5)$ across various regions of China. During the Winter Olympics observation period, the concentrations of NO_3 precursors (NO_2 and O_3) at this site were lower than those observed in rural areas, such as Wangdu in Hebei province (Wang et al., 2022). This discrepancy resulted in relatively lower calculated $P(NO_3)$ values, which ranged from 0.01 to 2.4 ppbv h^{-1}, with a mean value of 0.5 ± 0.4 ppbv h^{-1}. The average $P(NO_3)$ value observed in this study aligns with the data reported for summer at the Mount Tai site (0.45 ± 0.40 ppbv h^{-1}) and winter in the Beijing area (0.4 ppbv h^{-1}) (Wang et al., 2021, 2017d). However, these values are considerably lower than those observed in Beijing during autumn and in Taizhou during summer (Li et al., 2020; Wang et al., 2017b). In contrast to national statistics, the average $P(NO_3)$ value in this study is lower than the cold season (October-March) average for China, which stands at 0.67 ± 0.23 ppbv h^{-1} (Wang et al., 2023a).

Table 3. Summary of field-observed N_2O_5, NO_3, NO_2, and O_3 mixing ratios, $P(NO_3)$ and $\tau(N_2O_5)$.

Region	Location	Time	N_2O_5 (pptv)	NO_3 (pptv)	NO_2 (ppbv)	O_3 (ppbv)	$P(NO_3)$ (ppbv h^{-1})	$\tau(N_2O_5)$ (min)	References
Urban	Beijing	Sep-Oct, 2016	68.0 ± 136.7	-	35.1 ± 16.6	27.7 ± 25.2	2.25 ± 2.02	-	(Wang et al., 2017b)
Urban	Beijing	Nov-Dec, 2016	23.4 ± 25.9 (max 43.0)	0.04 ± 0.09	39.0 ± 17.8	16.6 ± 8.1	0.94 ± 0.83	2.5 ± 2.5	(Li et al., 2022)
Urban	Beijing	May-June, 2016	73 (max 937)	8 (max 133)	14.4	40.8	1.2 ± 0.9 (night)	270 ± 240 s	(Wang et al., 2018)
Urban	Shanghai	Aug-Oct, 2011	310 ± 380	16 ± 9 (max 95)	~76	23 ± 8 (max 57)	1.10 ± 1.09	-	(Wang et al., 2013)
Urban	Changzhou	May-June, 2019	53.4 ± 66.1 (max 304.7)	4.7 ± 3.5 (max 17.7)	13.7 ± 8.9	48.4 ± 27.8	1.7± 1.2 (night)	1.6 ± 1.5	(Lin et al., 2022)
Suburban	Taizhou	May-Jun, 2018	26.0 ± 35.7 (max 492)	4.4 ± 2.2 (max 29.3)	14.0 ± 10.0	48.2 ± 32.5	1.2 ± 0.3	0.93 ± 1.13	(Li et al., 2020)
Rural	Wangdu	Jun- July, 2014	30.5 ± 35.4 (max 429)	4.8 ± 3.3 (max 25)	9.6	54	1.03 ± 0.48	162 s	(Wang et al., 2022)
Mountain	Shandong	Jul- Aug, 2014	6. 8± 7.7 (max 167)	-	3 (night)	77 (night)	0.45 ± 0.40	1.2–1.3 (night)	(Wang et al., 2017d)

https://doi.org/10.5194/egusphere-2025-2210
Preprint. Discussion started: 17 June 2025

Region	Location	Time	N_2O_5 (pptv)	NO_3 (pptv)	NO_2 (ppbv)	O_3 (ppbv)	$P(NO_3)$ (ppbv h^{-1})	$\tau(N_2O_5)$ (min)	References
Urban	Beijing	Feb-Mar, 2022	86.7 ± 116.5	0.6 ± 0.7 (max 4.6)	14.8 ± 11.5	28.6 ± 12.8	0.5 ± 0.4	11.9 ± 11.8	This study

The relatively lower $P(NO_3)$ values in this study can be attributed to the lower temperatures, which reduce the reaction rate constants for NO_2 and O_3. For instance, under identical NO_2 and O_3 mixing ratios (NO_2=15 ppbv and O_3=30 ppbv), an increase in temperature from -1 °C to 5 °C leads to a corresponding increase in the reaction rate constant from 1.59×10^{-17} to 1.94×10^{-17}, resulting in a rise in $P(NO_3)$ from 0.70 ppbv h^{-1} to 0.83 ppbv h^{-1}. The temporal trend of $P(NO_3)$ during the POP exhibited a slight difference from that during the OGP, which can be attributed to fluctuations in temperature and precursor concentrations.

$\tau(N_2O_5)$ serves as an important parameter for delineating the sources and sinks of NO_x within a given region. It plays a crucial role in elucidating the chemical equilibrium dynamics of NO_3 and N_2O_5 at measurement sites and in evaluating the capacity for N_2O_5 removal. In this study, the observed $\tau(N_2O_5)$ is notably prolonged compared to those documented in Wangdu (77 s and 172 s) and Beijing (270 s) (Tham et al., 2016; Wang et al., 2018), yet they remain shorter than those of the measurements conducted in the Hong Kong boundary layer (Brown et al., 2016). This discrepancy underscores a diminished reactivity of NO_3-N_2O_5 at our study site during the observation window, leading to a more gradual overall depletion of NO_3 and N_2O_5.

$\tau(N_2O_5)$ varied significantly between the two periods, with nocturnal mean lifetime during the POP being approximately 5 minutes shorter than that recorded during the OGP. This observation points towards an intensified nocturnal depletion of NO_3 and N_2O_5 in the urban setting of Beijing, a phenomenon that will be subjected to a more in-depth analysis in the forthcoming discussion sections. Drawing from Eq. (3), it is evident that the disparities in the lifetimes mentioned above are primarily due to the variations in the concentration of N_2O_5 rather than merely alterations in $P(NO_3)$. A consistent correlation was observed, wherein elevated N_2O_5 concentrations were associated with extended lifetimes, highlighting the pivotal role of N_2O_5 concentration in modulating its own atmospheric persistence.

3.2 Mean diurnal variations

Figure 3 displays the average diurnal variations in NO, NO_2, N_2O_5, NO_3, O_3 mixing ratios, and the NO_3 production rate during the study period. Specifically, panel (a) presents the daily mean patterns for the OGP, whereas panel (b) depicts those for the POP. Notable differences in concentration but similar diurnal trends were observed between the two periods.

https://doi.org/10.5194/egusphere-2025-2210
Preprint. Discussion started: 17 June 2025

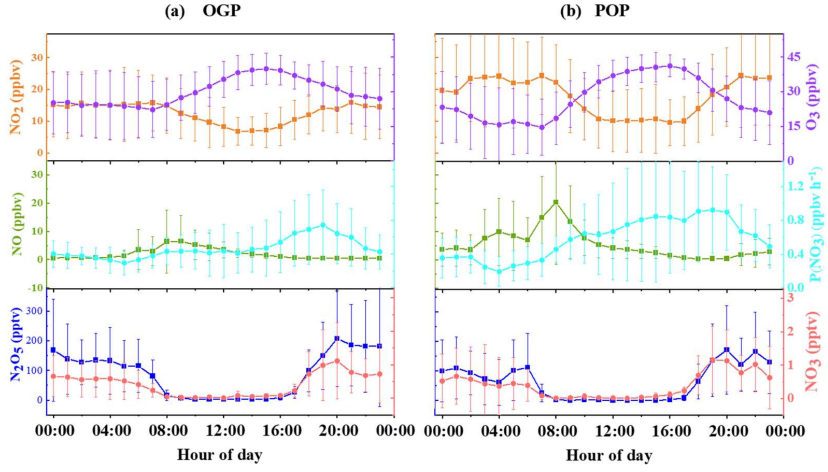

Figure 3. Mean diurnal variations in NO, NO_2, N_2O_5, NO_3, O_3 mixing ratios and $P(NO_3)$ during and after the 2022 Beijing Winter Olympics

In urban Beijing, nocturnal NO mixing ratios were substantially lower during the OGP compared to the POP. NO concentrations exhibited a gradual increase after midnight, attaining the first peak value of 3.5 ppbv at 06:00. A secondary peak occurred during morning rush hour (08:00 LST), reaching 20.4 ppbv during the POP. O_3 mixing ratio exhibited a characteristic mid-afternoon peak, rising progressively after sunrise to a maximum of 41.2 ppbv between 15:00-16:00, followed by a gradual nocturnal decline to the minimum mixing ratio around 07:00. Notably, nocturnal O_3 levels during the POP were markedly lower than those during the OGP, indicating enhanced O_3 titration by elevated NO concentrations. This process contributed to maintaining lower nighttime O_3 levels while concurrently generating higher NO_2 concentrations during the POP compared to the OGP.

From the daily average variation perspective, the trends of NO_2 and O_3 mixing ratios exhibited an inverse correlation, consistent with previous studies (Wang et al., 2020). Nocturnal NO_2 concentrations substantially surpassed daytime levels. Furthermore, due to NO titration of NO_3 (R4), $P(NO_3)$ showed a strong negative correlation with NO (Fig. S1). The highest value of $P(NO_3)$ in both periods occurred at 19:00, with values of 0.74 ppbv h^{-1} and 0.92 ppbv h^{-1}, respectively, both slightly lower than those observed in the North China Plain (1 ~ 2 ppbv h^{-1}) (Wang et al., 2022, 2018). The daily average values of $P(NO_3)$ during the POP and the OGP were 0.5 ppbv h^{-1} and 0.6 ppbv h^{-1}, respectively. Following the conclusion of the Winter Olympics, increased primary pollutant concentrations led to elevated $P(NO_3)$, with the concentrations of NO_3 and N_2O_5 expected to rise amidst constant losses.

The diurnal variations in N_2O_5 and NO_3 mixing ratios exhibited comparable patterns across both periods. Specifically, both species exhibited rapid accumulation after sunset, reaching peak values around 20:00 (208.2 pptv in OGP vs. 171.2 pptv in POP). Subsequently, due to constrained NO emissions and a reduction in $P(NO_3)$,

https://doi.org/10.5194/egusphere-2025-2210
Preprint. Discussion started: 17 June 2025

their concentrations gradually decreased prior to midnight, eventually reaching detection limits by sunrise. However, during the POP, specifically from 02:00 to 04:00, elevated nocturnal NO emissions triggered a precipitous drop in N_2O_5 and NO_3 concentrations. This decline was further exacerbated by the ensuing titration reaction of NO, which led to a rapid decrease in O_3 concentration, thereby fostering higher NO_2 levels and an uptick in $P(NO_3)$. Around 06:00, another N_2O_5 concentration peak was observed at 112.1 pptv. NO_3 exhibited a similar trend, peaking at 1.1 pptv between 19:00 and 20:00. The daily average variation trends of both N_2O_5 and NO_3 aligned with those reported for the Yangtze River Delta and North China regions (Li et al., 2020; Wang et al., 2022, 2017c; Xia et al., 2021). While the chemical conditions in this study bore similarities to those in summer Beijing, the meteorological conditions differed, notably characterized by higher relative humidity during the summer. The average nocturnal N_2O_5 concentration over the observation period was 113.7 ± 103.3 pptv, which was higher than that observed in the Changping area of Beijing (Wang et al., 2018), indicating that the loss process of NO_3 and N_2O_5 in Beijing during winter is more sluggish compared to that in the summer.

4 Discussion

4.1. The lifetime of N_2O_5

RH and S_a are pivotal factors influencing $\tau(N_2O_5)$ (Brown et al., 2017; Lin et al., 2022). The correlation between these parameters and $\tau(N_2O_5)$ is presented in Fig. 4. As shown in Fig. 4(a), $\tau(N_2O_5)$ exhibited an increasing trend with RH when RH was below 35 %. However, substantial deviations in this relationship suggests complex underlying processes. When RH exceeded 35 %, $\tau(N_2O_5)$ decreased with increasing humidity. Specifically, at RH > 60 %, $\tau(N_2O_5)$ approached zero, indicative of high-humidity conditions such as rain or snow. This strong RH dependence highlights the importance of heterogeneous N_2O_5 uptake in urban Beijing, potentially dominating NO_3 loss pathways under elevated RH. The rationale for this is twofold: (1) hygroscopic aerosols grow at higher RH, increasing their specific surface area and thus reactive sites for N_2O_5 uptake; (2) this hygroscopic growth likely enhances the efficiency of heterogeneous reactions involving N_2O_5, accelerating its loss (Brown et al., 2016).

Figure 4(b) illustrates that the mean $\tau(N_2O_5)$ gradually increases from ~10 to 15 minutes as S_a rises to 280 μm² cm⁻³. However, beyond this S_a value, $\tau(N_2O_5)$ remained at a relatively stable but slightly decreasing value (< 15 min) despite continued growth in S_a. While this declining trend in $\tau(N_2O_5)$ with increasing S_a aligns with previous findings (Lin et al., 2022; Wang et al., 2020; Zhou et al., 2018), quantitative discrepancies in the observed values warrant note. When S_a ranges from 450 to 1000 μm² cm⁻³, a robust negative correlation between $\tau(N_2O_5)$ and S_a emerged. The joint dependence of $\tau(N_2O_5)$ on RH and S_a underscores the critical role of N_2O_5 heterogeneous uptake on particle surfaces in mediating NO_3 and N_2O_5 loss pathways. Under high-RH conditions, this process may dominate due to enhanced hygroscopic particle growth, which increases reactive surface area and facilitates N_2O_5 hydrolysis (Brown et al., 2016; Brown and Stutz, 2012; Chang et al., 2011).

https://doi.org/10.5194/egusphere-2025-2210
Preprint. Discussion started: 17 June 2025

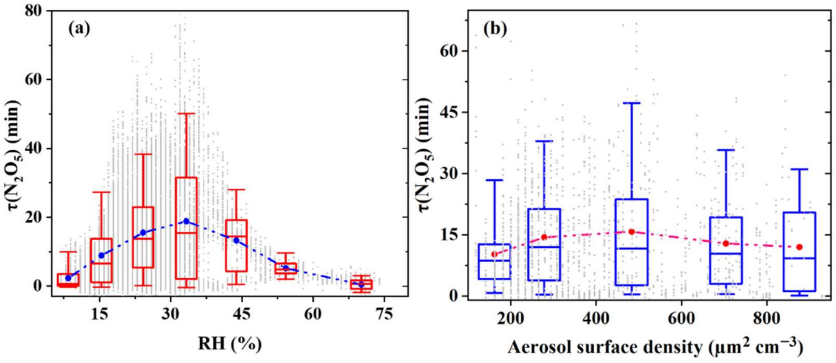

Figure 4. The relationship between τ(N_2O_5) and S_a as well as RH during the observation period.

4.2 NO_3 and N_2O_5 pathways

4.2.1 Loss of NO_3 via reaction with VOCs and N_2O_5 uptake coefficients

To gain a deeper insight into the loss mechanisms of NO_3 and N_2O_5, the total reactivity of NO_3 was computed by employing Equation (4) in Section 2.3. A comprehensive array of 99 distinct VOCs was detected at this site. The reaction rate constants for the interaction between VOCs and the oxidizing agent NO_3 were obtained from the literature (Atkinson and Arey, 2003; Brown et al., 2011) or extracted from the National Institute of Standards and Technology database (accessible via http://webbook.nist.gov/chemistry/). For certain VOC species where quantitative laboratory reaction rate constants were unavailable, these values were estimated based on the reaction rate constants of analogous species.

A detailed examination of the observational data disclosed that the VOCs with the highest concentrations were predominantly anthropogenic VOCs (AVOCs), including ethane, propane, acetone, acetylene, and ethylene. Despite their elevated concentrations, their low reaction rate constants with NO_3 resulted in negligible contributions to k_{NO_3}, thereby indicating that they were not primary reactants. The observational data for Biogenic VOCs (BVOCs) solely comprised isoprene, with an average concentration of 0.016 ppbv. Nevertheless, owing to its comparatively high reaction rate with NO_3, isoprene emerged as a significant contributor to the NO_3 loss pathway associated with VOCs. The statistical data pertaining to VOC concentrations and reaction rates are provided in Table S1.

Figure 5 presents a detailed visualization of the reactivity and relative contribution of diverse VOC categories to NO_3 reactions across two periods. It revealed that AVOCs dominated nocturnal VOC-NO_3 reaction dynamics, accounting for nearly 70 % of the total reactivity during both the OGP and POP. This result aligned harmoniously with observations from other urban environments (Lin et al., 2022). The NO_3-oxidized VOC landscape in Beijing was predominantly characterized by styrene and isoprene, with average reactivity values of 0.34×10^{-3} s^{-1} and 0.25×10^{-3} s^{-1}, respectively. Isoprene in urban Beijing exhibits dual anthropogenic and

https://doi.org/10.5194/egusphere-2025-2210
Preprint. Discussion started: 17 June 2025

biogenic sources: traffic emissions (e.g., gasoline exhaust) dominate anthropogenic contributions, while plant emissions (e.g., deciduous and evergreen species) constitute the primary biogenic source. Remarkably, biogenic isoprene concentrations significantly outstrip those from traffic emissions (Cheng et al., 2018; Yuan et al., 2009). Styrene emissions in Beijing are predominantly linked to vehicle exhaust, though natural emissions from evergreen and oleander species also contribute (Hu et al., 2023; Li et al., 2014). Other AVOCs also contribute to k_{NO_3}, with an average reactivity of 0.26×10^{-3} s^{-1}. When ranked by relative contribution, the dominant AVOCs following the order: butene, butadiene, and propylene (Fig. S2). However, the reactivity estimates for BVOCs may be underestimated, as observational data for key BVOCs (e.g., limonene, α-pinene) were unavailable in this study.

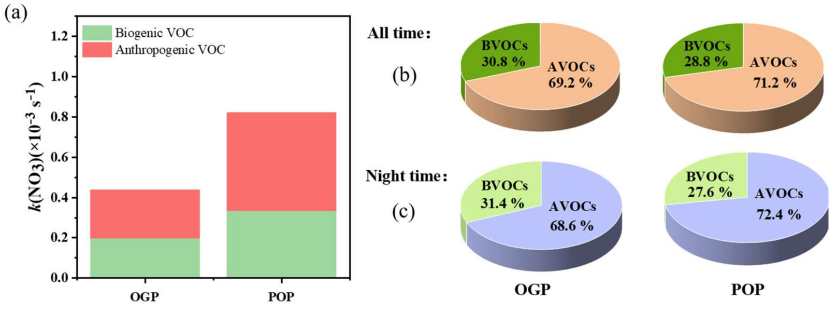

Figure 5. The changes in reactivity and relative contribution of AVOCs and BVOCs at different periods.

As shown in Fig. 5(a), the reactivity of VOCs with NO_3 underwent a marked escalation after the conclusion of the Winter Olympics, surging from 0.44×10^{-3} s^{-1} to 0.82×10^{-3} s^{-1}. The upsurge is primarily driven by elevated VOCs concentrations following the cessation of emission reduction measures (Table S1). Statistical analyses indicated a substantial surge in AVOCs concentrations, which accounted for 72.4 % of nocturnal reactivity during POP. In contrast, BVOCs reactivity showed limited growth, resulting in a decreased BVOCs contribution (28.8 % during the POP, down from 31.4 % to 27.6 %; Fig. 5c). Based on the aforementioned analysis, VOCs concentrations remained low during the winter observation period, predominantly stemming from transportation emissions. Stringent emission controls implemented during this period suppressed VOC emissions, thereby reducing NO_3-VOC reactivity and diminishing their role in NO_3 radical removal. The post-Olympic relaxation of these controls led to a rebound in AVOC levels, reasserting their dominance in nocturnal NO_3 reactivity.

For the quantification of $k_{N_2O_5}$, the $\gamma(N_2O_5)$ must first be determined and subsequently calculated according to Eq. (6). The methodology for determining $\gamma(N_2O_5)$ is elaborated in Section 2.3, and the calculation results for S_a are presented in Fig. S3. To mitigate the interference of water vapor and NO concentrations on the steady-state equilibrium, data fitting was constrained to periods with RH < 70 % and NO mixing ratios < 1 ppbv. For each day, the slope of the linear regression yielded the $\gamma(N_2O_5)$, while the intercept represented k_{NO_3}. Due to

https://doi.org/10.5194/egusphere-2025-2210
Preprint. Discussion started: 17 June 2025

variations in the composition and concentration of VOCs, which can alter k_{NO_3}, negative intercept values occasionally occurred during fitting, contradicting physical feasibility. Such cases were excluded from analysis, yielding 23 valid data points. The derived $\gamma(N_2O_5)$ values were provided in Table S2 and exhibited substantial variation under different environmental conditions. Specifically, under rainy or snowy conditions with elevated RH, $\gamma(N_2O_5)$ would reach as high as 0.22. For most of the time, $\gamma(N_2O_5)$ fluctuated between 0.01 and 0.12, with an average uptake coefficient of 0.032 ± 0.049. When compared to ground-based N_2O_5 uptake coefficients observed in other regions of China and other countries, the values derived in this study align with those reported in Beijing (0.01–0.09) (Li et al., 2022; Wang et al., 2017b; Zhou et al., 2018; Xia et al., 2021), but exceed those in Wangdu (0.006–0.034) (Tham et al., 2018), Hong Kong (0.014 ± 0.007) (Brown et al., 2016), Germany (0.028 ± 0.029), and measurements from the United States (0.008–0.04) (Mielke et al., 2013; Phillips et al., 2016).

4.2.2 Time-series variations in NO_3 and N_2O_5 reactivities

The time series of k_{NO_3} derived from Eq. (4) is presented in Fig. 6. By comparing reaction pathways, NO_3 was found to predominantly react with NO, with an average reaction rate of 2.54 s^{-1}. Following this, the most notable reaction was the heterogeneous reaction of N_2O_5, with an average loss rate of 0.20 ± 0.63 s^{-1}. During the high-humidity night of February 13, the heterogeneous reactivity of N_2O_5 surged to 2.35 s^{-1}. A comprehensive summary of nocturnal mean reactivities is provided in Table 4.

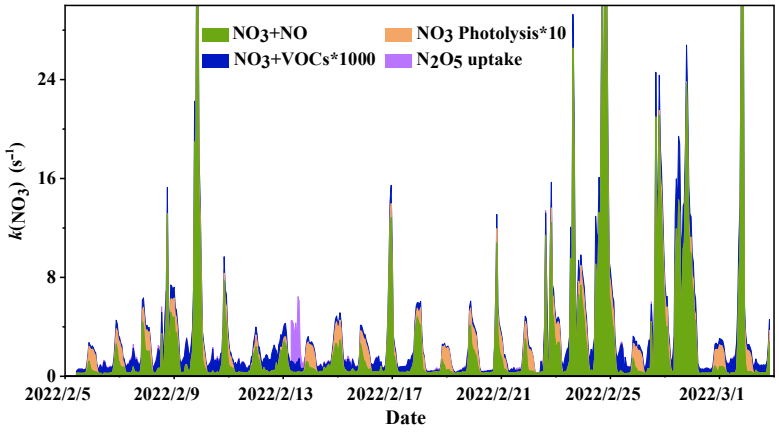

Figure 6. Time series variation of k_{NO_3} (reactions with NO and VOCs, homogeneous uptake of N_2O_5 and photolysis of NO_3).

A significant uptick in k_{NO_3} was observed after the end of the Winter Olympics, escalating from 1.14 s^{-1} to 3.06 s^{-1}. This surge suggests an augmentation in the nocturnal NO_3 loss, coinciding with the relaxation of emission control measures. Concurrently, the reactivity of NO_3 with NO also witnessed a substantial rise, from 0.81 s^{-1} to 3.00 s^{-1}. This enhancement can be attributed to the heightened primary NO emissions due to the cessation of

https://doi.org/10.5194/egusphere-2025-2210
Preprint. Discussion started: 17 June 2025

Winter Olympics-related control measures, coupled with an accelerated loss of NO_3 through the temperature-dependent acceleration of the NO_3+NO reaction. In a parallel trend, the reactivity of VOCs also exhibited an increase, escalating from 0.8×10^{-3} s^{-1} to 1.4×10^{-3} s^{-1}. During the POP, the N_2O_5 removal rate declined relative to the OGP. This reduction is attributed to lower RH, which diminished S_a availability for heterogeneous uptake despite stable aerosol mass concentrations. Lower RH suppressed N_2O_5 hydrolysis, thereby reducing its contribution to NO_3 loss.

Table 4 Statistics of k_{NO_3} across various pathways and time periods

k_{NO_3} (s^{-1})	OGP	POP
NO_3+NO	0.81	3.00
NO_3+VOCs	0.8×10^{-3}	1.4×10^{-3}
N_2O_5 uptake	0.32	0.06
Total	1.14	3.06

4.2.3 The NO_3 loss budget

Figure 7 shows the diurnal variations and relative contributions of NO_3 loss pathways. The average NO_3 removal rate increased from 1.14 ppbv h^{-1} during the OGP to 1.61 ppbv h^{-1} during POP, reflecting the relaxation of emission controls. During the OGP, the NO_3 + NO reaction activity exhibited a pronounced morning peak (96.7 % of the total k_{NO_3}) at 07:00 local time, coinciding with morning rush-hour NO emission maxima. In contrast, the POP featured a reconfigured diurnal pattern, with the NO–NO_3 reaction activity intensifying nocturnally and peaking at 2.04 ppbv h^{-1} at 22:00, accounting for 89.2 % of the NO_3 loss (Fig. S4).

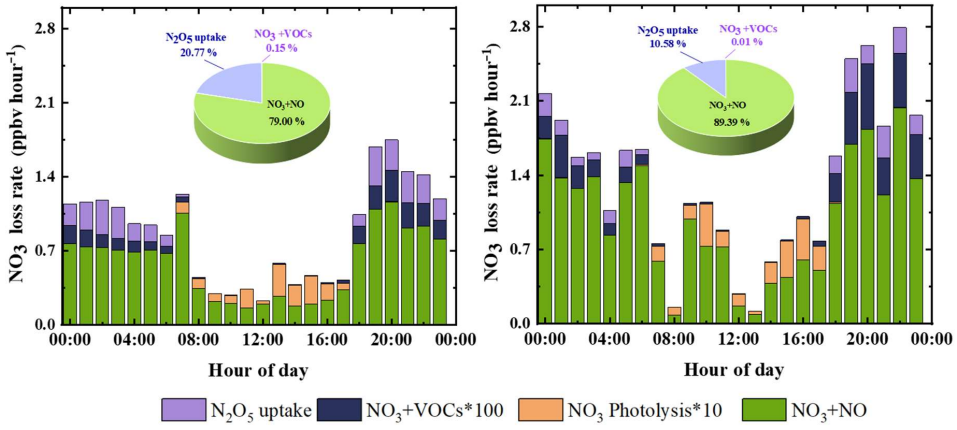

Figure 7. Mean daily variation and reactivity share of different loss pathways.

The heterogeneous N_2O_5 uptake pathway, an indirect nocturnal sink, displayed a gradual post-sunset increase in removal rate, peaking at 0.33 ppbv h^{-1} at 19:00 before declining. This pathway contributed 20.8 % of total

https://doi.org/10.5194/egusphere-2025-2210
Preprint. Discussion started: 17 June 2025

NO_3 loss during the OGP, comparable to urban Beijing (Li et al., 2022). However, its contribution diminished to 10.6 % during the POP due to lower RH, which reduced S_a availability for uptake. Similarly, the nocturnal reaction rate between NO_3 and VOCs exhibited a gradual increase after sunset, reaching its peak value of approximately 0.004 ppbv h^{-1} after 20:00. This trend is consistent with the observation in suburban Yangtze River Delta and urban Beijing (Hu et al., 2023; Wang et al., 2020) but is significantly lower than winter urban sites in Beijing (0.22 ppbv h^{-1}) (Hu et al., 2023) and Changzhou (0.18 ppbv h^{-1}) (Lin et al., 2022). The maximum VOC reactivity contribution to NO_3 loss was only 0.5 %, far below the 36.4 % reported for Taizhou, Jiangsu (Wang et al., 2020), likely due to lower VOC reactivity in winter.

While NO_3 removal in both periods was predominantly driven by reactions with NO (Fig. 7), the relative contributions of competing reaction pathways exhibited notable variations. During the OGP, NO_3 + NO reactions accounted for 79.0 % of total NO_3 removal (down from 89.4 % in the POP), reflecting reduced NO emissions under control measures. In contrast, the POP saw NO_3 + NO reactivity dominate (up to 96.8 % of NO_3 loss), exceeding the 65 % maximum observed in urban Beijing (Li et al., 2022). The N_2O_5 heterogeneous pathway's contribution (20.8 % during OGP) underscores its potential as a significant nocturnal NO_3 sink under reduced NO emissions.

5 Summary and conclusions

This study presents a comprehensive characterization of nocturnal NO_3–N_2O_5 chemistry during the 2022 Beijing Winter Olympics. The average N_2O_5 concentration was 86.7 pptv, peaking at 874.9 pptv, while maximum calculated NO_3 concentrations reached 4.6 pptv. The mean $P(NO_3)$ value was 0.5 ± 0.4 ppbv h^{-1}, aligning with previous winter observations in Beijing, peaking at 2.4 ppbv h^{-1}, which reflects the region's enhanced nocturnal oxidative capacity. The average steady-state lifetime of N_2O_5 was 11.9 ± 11.8 minutes, which was longer than values reported for summer in Beijing, suggesting a slower nocturnal NO_3 loss rate in winter.

NO was the dominant sink for NO_3 throughout the observation period, contributing up to 89.2% of its total loss, while VOCs played a negligible role (approximately 0.1 %). Among VOCs, anthropogenic species (AVOCs) exhibited relatively high reactivity, with styrene identified as the most reactive compound. Steady-state calculations of the N_2O_5 heterogeneous uptake coefficient yielded values ranging from 0.01 to 0.1, comparable to observations in Beijing and Wangdu. Under high relative humidity, the contribution of heterogeneous N_2O_5 uptake to NO_3 loss increased notably.

After the Winter Olympics, the lifetime of N_2O_5 decreased by approximately 5 minutes, indicating an enhanced nocturnal NO_3 loss rate. This trend was primarily driven by an increase in the k_{NO_3}. During the 2022 Beijing Winter Olympics, heterogeneous uptake of N_2O_5 contributed up to 20.8 % of total NO_3 loss, underscoring its significance as a nocturnal NO_3 removal pathway under emission mitigation strategies. This finding underscores

https://doi.org/10.5194/egusphere-2025-2210
Preprint. Discussion started: 17 June 2025

the growing role of heterogeneous chemistry in urban NO_3 cycling as primary NO and VOC emissions decline. The findings offer new insights into how emission control measures shape nighttime oxidation processes in a polluted urban environment. Future studies incorporating detailed measurements of VOC components could further reveal the response of regional air quality to nocturnal oxidation mechanisms.

Data availability. Data are available at https://doi.org/10.5281/zenodo.15381990 (T. Zhang et al., 2025).

Supplement. The following file is available free of charge. Supplement of "Measurement report: Variations and environmental impacts of atmospheric N_2O_5 concentrations in urban Beijing during the 2022 Winter Olympics"

Author Contributions. TZ, WL, and CY designed the research. WL, and CY organized this field campaign. TZ, PZ, YC, TL and LZ carried out the field measurements and provided the field measurement dataset. TZ performed data analysis, interpreted the data and wrote the manuscript with revision mainly from WL. All authors have given approval to the final version of the manuscript.

Competing interests. The contact author has declared that none of the authors has any competing interests.

Disclaimer. Publisher's note: Copernicus Publications remains neutral with regard to jurisdictional claims in published maps and institutional affiliations.

Acknowledgment. The authors would like to thank the field campaign team for the data that they contributed during the 2022 Beijing Winter Olympics.

Financial support. This study was financially supported by the National Natural Science Foundation of China (42405083), the National Key Research and Development Program (2024YFC3711902).

References

Atkinson, R. and Arey, J.: Atmospheric Degradation of Volatile Organic Compounds, Chem. Rev., 103, 4605–4638, https://doi.org/10.1021/cr0206420, 2003.

Bertram, T. H., Thornton, J. A., Riedel, T. P., Middlebrook, A. M., Bahreini, R., Bates, T. S., Quinn, P. K., and Coffman, D. J.: Direct observations of N_2O_5 reactivity on ambient aerosol particles, Geophys. Res. Lett., 36, L19803, https://doi.org/10.1029/2009GL040248, 2009.

Brown, S. S. and Stutz, J.: Nighttime radical observations and chemistry, Chem. Soc. Rev., 41, 6405, https://doi.org/10.1039/c2cs35181a, 2012.

Brown, S. S., Dubé, W. P., Peischl, J., Ryerson, T. B., Atlas, E., Warneke, C., de Gouw, J. A., te Lintel Hekkert, S., Brock, C. A., Flocke, F., Trainer, M., Parrish, D. D., Feshenfeld, F. C., and Ravishankara, A. R.: Budgets for nocturnal VOC oxidation by nitrate radicals aloft during the 2006 Texas Air Quality Study, J. Geophys.

https://doi.org/10.5194/egusphere-2025-2210
Preprint. Discussion started: 17 June 2025

Res., 116, 1–15, https://doi.org/10.1029/2011JD016544, 2011.

Brown, S. S., Dubé, W. P., Tham, Y. J., Zha, Q., Xue, L., Poon, S., Wang, Z., Blake, D. R., Tsui, W., Parrish, D. D., and Wang, T.: Nighttime chemistry at a high altitude site above Hong Kong, J. Geophys. Res. Atmos., 121, 2457–2475, https://doi.org/10.1002/2015JD024566, 2016.

Brown, S. S., An, H., Lee, M., Park, J.-H., Lee, S.-D., Fibiger, D. L., McDuffie, E. E., Dubé, W. P., Wagner, N. L., and Min, K.-E.: Cavity enhanced spectroscopy for measurement of nitrogen oxides in the Anthropocene: results from the Seoul tower during MAPS 2015, Faraday Discuss., 200, 529–557, https://doi.org/10.1039/C7FD00001D, 2017.

Chang, W. L., Bhave, P. V., Brown, S. S., Riemer, N., Stutz, J., and Dabdub, D.: Heterogeneous Atmospheric Chemistry, Ambient Measurements, and Model Calculations of N_2O_5: A Review, Aerosol Sci. Technol., 45, 665–695, https://doi.org/10.1080/02786826.2010.551672, 2011.

Cheng, X., Li, H., Zhang, Y., and Li, Y.: Atmospheric isoprene and monoterpenes in a typical urban area of Beijing: Pollution characterization, chemical reactivity and source identification, J. Environ. Sci., 71, 150–167, https://doi.org/10.1016/j.jes.2017.12.017, 2018.

Crutzen, P. J.: The Role of NO and NO_2 in the Chemistry of the Troposphere and Stratosphere, Annu. Rev. Earth Planet. Sci., 7, 443–472, https://doi.org/10.1146/annurev.ea.07.050179.002303, 1979.

Fry, J. L. and Sackinger, K.: Model investigation of NO_3 secondary organic aerosol (SOA) source and heterogeneous organic aerosol (OA) sink in the western United States, Atmos. Chem. Phys., 12, 8797–8811, https://doi.org/10.5194/acp-12-8797-2012, 2012.

Hoyle, C. R., Berntsen, T., Myhre, G., and Isaksen, I. S. A.: Secondary organic aerosol in the global aerosol - chemical transport model Oslo CTM2, Atmos. Chem. Phys., 7, 5675–5694, https://doi.org/10.5194/acp-7-5675-2007, 2007.

Hu, H., Wang, H., Lu, K., Wang, J., Zheng, Z., Xu, X., Zhai, T., Chen, X., Lu, X., Fu, W., Li, X., Zeng, L., Hu, M., Zhang, Y., and Fan, S.: Variation and trend of nitrate radical reactivity towards volatile organic compounds in Beijing, China, Atmos. Chem. Phys. Chem. Phys., 23, 8211–8223, https://doi.org/10.5194/acp-23-8211-2023, 2023.

Huang Z., Hu W., Jin R., Hou S., LI P., Bi K., He C., Wang Y., Duan P., Liu D., Wu L., Deng J., Sun Y., and Fu P.: Chemical composition and sources of fine particles in Beijing around the Winter Olympics, China Environ. Sci., 44, 5344–5356, https://doi.org/10.19674/j.cnki.issn1000-6923.20240604.002, 2024.

Li, H., Zheng, B., Lei, Y., Hauglustaine, D., Chen, C., Lin, X., Zhang, Y., Zhang, Q., and He, K.: Trends and drivers of anthropogenic NO_x emissions in China since 2020, Environ. Sci. Ecotechnol., 21, 100425, https://doi.org/10.1016/j.ese.2024.100425, 2024.

Li, L., Li, H., and Zhang, X.: Pollution characteristics and health risk assessment of benzene homologues in ambient air in the northeastern urban area of Beijing, China, J. Environ. Sci., 26, 214–223, https://doi.org/10.1016/S1001-0742(13)60400-3, 2014.

Li, Z., Hu, R., Xie, P., Wang, H., Lu, K., and Wang, D.: Intercomparison of in situ CRDS and CEAS for measurements of atmospheric N_2O_5 in Beijing, China, Sci. Total Environ., 613–614, 131–139,

https://doi.org/10.5194/egusphere-2025-2210
Preprint. Discussion started: 17 June 2025

https://doi.org/10.1016/j.scitotenv.2017.08.302, 2018.

Li, Z., Xie, P., Hu, R., Wang, D., Jin, H., Chen, H., Lin, C., and Liu, W.: Observations of N_2O_5 and NO_3 at a suburban environment in Yangtze river delta in China: Estimating heterogeneous N_2O_5 uptake coefficients, J. Environ. Sci., 95, 248–255, https://doi.org/10.1016/j.jes.2020.04.041, 2020.

Li, Z., Wang, D., Xie, P., Hu, R., chen, H., and Lin, C.: Nighttime N_2O_5 chemistry in an urban site of Beijing in winter based on the measurements by cavity ring-down spectroscopy, Air Qual. Atmos. Hlth, 15, 867–876, https://doi.org/10.1007/s11869-021-01125-4, 2022.

Lin, C., Hu, R., Xie, P., Lou, S., Zhang, G., Tong, J., Liu, J., and Liu, W.: Nocturnal atmospheric chemistry of NO_3 and N_2O_5 over Changzhou in the Yangtze River Delta in China, J. Environ. Sci., 114, 376–390, https://doi.org/10.1016/j.jes.2021.09.016, 2022.

Lu, X., Qin, M., Xie, P., Duan, J., Fang, W., and Liu, W.: Observation of ambient NO_3 radicals by LP-DOAS at a rural site in North China Plain, Sci. Total Environ., 804, 149680, https://doi.org/10.1016/j.scitotenv.2021.149680, 2022.

Mielke, L. H., Stutz, J., Tsai, C., Hurlock, S. C., Roberts, J. M., Veres, P. R., Froyd, K. D., Hayes, P. L., Cubison, M. J., Jimenez, J. L., Washenfelder, R. A., Young, C. J., Gilman, J. B., de Gouw, J. A., Flynn, J. H., Grossberg, N., Lefer, B. L., Liu, J., Weber, R. J., and Osthoff, H. D.: Heterogeneous formation of nitryl chloride and its role as a nocturnal NO_x reservoir species during CalNex-LA 2010, J. Geophys. Res. Atmos., 118, 10,638-10,652, https://doi.org/10.1002/jgrd.50783, 2013.

Ng, N. L., Brown, S. S., Archibald, A. T., Atlas, E., Cohen, R. C., Crowley, J. N., Day, D. A., Donahue, N. M., Fry, J. L., Fuchs, H., Griffin, R. J., Guzman, M. I., Herrmann, H., Hodzic, A., Iinuma, Y., Jimenez, J. L., Kiendler-Scharr, A., Lee, B. H., Luecken, D. J., Mao, J., McLaren, R., Mutzel, A., Osthoff, H. D., Ouyang, B., Picquet-Varrault, B., Platt, U., Pye, H. O. T., Rudich, Y., Schwantes, R. H., Shiraiwa, M., Stutz, J., Thornton, J. A., Tilgner, A., Williams, B. J., and Zaveri, R. A.: Nitrate radicals and biogenic volatile organic compounds: oxidation, mechanisms, and organic aerosol, Atmos. Chem. Phys., 17, 2103–2162, https://doi.org/10.5194/acp-17-2103-2017, 2017.

Osthoff, H. D., Sommariva, R., Baynard, T., Pettersson, A., Williams, E. J., Lerner, B. M., Roberts, J. M., Stark, H., Goldan, P. D., Kuster, W. C., Bates, T. S., Coffman, D., Ravishankara, A. R., and Brown, S. S.: Observation of daytimeN_2O_5 in the marine boundary layer during New England Air Quality Study–Intercontinental Transport and Chemical Transformation 2004, J. Geophys. Res. Atmos., 111, https://doi.org/10.1029/2006JD007593, 2006.

Phillips, G. J., Thieser, J., Tang, M., Sobanski, N., Schuster, G., Fachinger, J., Drewnick, F., Borrmann, S., Bingemer, H., Lelieveld, J., and Crowley, J. N.: Estimating N_2O_5 uptake coefficients using ambient measurements of NO_3, N_2O_5, $ClNO_2$ and particle-phase nitrate, Atmos. Chem. Phys., 16, 13231–13249, https://doi.org/10.5194/acp-16-13231-2016, 2016.

Pye, H. O. T., Chan, A. W. H., Barkley, M. P., and Seinfeld, J. H.: Global modeling of organic aerosol: the importance of reactive nitrogen (NO_x and NO_3), Atmos. Chem. Phys., 10, 11261–11276, https://doi.org/10.5194/acp-10-11261-2010, 2010.

https://doi.org/10.5194/egusphere-2025-2210
Preprint. Discussion started: 17 June 2025

Tang, M. J., Schuster, G., and Crowley, J. N.: Heterogeneous reaction of N_2O_5 with illite and Arizona test dust particles, Atmos. Chem. Phys., 14, 245–254, https://doi.org/10.5194/acp-14-245-2014, 2014.

Tham, Y. J., Wang, Z., Li, Q., Yun, H., Wang, W., Wang, X., Xue, L., Lu, K., Ma, N., Bohn, B., Li, X., Kecorius, S., Größ, J., Shao, M., Wiedensohler, A., Zhang, Y., and Wang, T.: Significant concentrations of nitryl chloride sustained in the morning: investigations of the causes and impacts on ozone production in a polluted region of northern China, Atmos. Chem. Phys., 16, 14959–14977, https://doi.org/10.5194/acp-16-14959-2016, 2016.

Tham, Y. J., Wang, Z., Li, Q., Wang, W., Wang, X., Lu, K., Ma, N., Yan, C., Kecorius, S., Wiedensohler, A., Zhang, Y., and Wang, T.: Heterogeneous N_2O_5 uptake coefficient and production yield of $ClNO_2$ in polluted northern China: Roles of aerosol water content and chemical composition, Atmos. Chem. Phys. Discuss., 1–10, https://doi.org/10.5194/acp-2018-313, 2018.

Wang, D., Xie, P., Hu, R., Li, Z., Chen, H., and Jin, H.: Reactivity and Loss Mechanisms of NO_3 and N_2O_5 at a Rural Site on the North China Plain, Atmos., 13, 1268, https://doi.org/10.3390/atmos13081268, 2022.

Wang, H., Chen, J., and Lu, K.: Development of a portable cavity-enhanced absorption spectrometer for the measurement of ambient NO_3 and N_2O_5: experimental setup, lab characterizations, and field applications in a polluted urban environment, Atmos. Meas. Tech., 10, 1465–1479, https://doi.org/10.5194/amt-10-1465-2017, 2017a.

Wang, H., Lu, K., Chen, X., Zhu, Q., Chen, Q., Guo, S., Jiang, M., Li, X., Shang, D., Tan, Z., Wu, Y., Wu, Z., Zou, Q., Zheng, Y., Zeng, L., Zhu, T., Hu, M., and Zhang, Y.: High N_2O_5 Concentrations Observed in Urban Beijing: Implications of a Large Nitrate Formation Pathway, Environ. Sci. Technol. Lett., 4, 416–420, https://doi.org/10.1021/acs.estlett.7b00341, 2017b.

Wang, H., Lu, K., Guo, S., Wu, Z., Shang, D., Tan, Z., Wang, Y., Le Breton, M., Lou, S., Tang, M., Wu, Y., Zhu, W., Zheng, J., Zeng, L., Hallquist, M., Hu, M., and Zhang, Y.: Efficient N_2O_5 uptake and NO_3 oxidation in the outflow of urban Beijing, Atmos. Chem. Phys., 18, 9705–9721, https://doi.org/10.5194/acp-18-9705-2018, 2018.

Wang, H., Chen, X., Lu, K., Hu, R., Li, Z., Wang, H., Ma, X., Yang, X., Chen, S., Dong, H., Liu, Y., Fang, X., Zeng, L., Hu, M., and Zhang, Y.: NO_3 and N_2O_5 chemistry at a suburban site during the EXPLORE-YRD campaign in 2018, Atmos. Environ., 224, 117180, https://doi.org/10.1016/j.atmosenv.2019.117180, 2020.

Wang, H., Wang, H., Lu, X., Lu, K., Zhang, L., Tham, Y. J., Shi, Z., Aikin, K., Fan, S., Brown, S. S., and Zhang, Y.: Increased night-time oxidation over China despite widespread decrease across the globe, Nat. Geosci., 16, 217–223, https://doi.org/10.1038/s41561-022-01122-x, 2023a.

Wang, J., Wang, H., Tham, Y. J., Ming, L., Zheng, Z., Fang, G., Sun, C., Ling, Z., Zhao, J., and Fan, S.: Measurement report: Atmospheric nitrate radical chemistry in the South China Sea influenced by the urban outflow of the Pearl River Delta, Atmos. Chem. Phys., 24, 977–992, https://doi.org/10.5194/acp-24-977-2024, 2024.

Wang, M., Zeng, L., Lu, S., Shao, M., Liu, X., Yu, X., Chen, W., Yuan, B., Zhang, Q., Hu, M., and Zhang, Z.: Development and validation of a cryogen-free automatic gas chromatograph system (GC-MS/FID) for

https://doi.org/10.5194/egusphere-2025-2210
Preprint. Discussion started: 17 June 2025

online measurements of volatile organic compounds, Anal Methods, 6, 9424–9434, https://doi.org/10.1039/C4AY01855A, 2014.

Wang, S., Shi, C., Zhou, B., Zhao, H., Wang, Z., Yang, S., and Chen, L.: Observation of NO_3 radicals over Shanghai, China, Atmos. Environ., 70, 401–409, https://doi.org/10.1016/j.atmosenv.2013.01.022, 2013.

Wang, X., Wang, H., Xue, L., Wang, T., Wang, L., Gu, R., Wang, W., Tham, Y. J., Wang, Z., Yang, L., Chen, J., and Wang, W.: Observations of N_2O_5 and $ClNO_2$ at a polluted urban surface site in North China: High N_2O_5 uptake coefficients and low $ClNO_2$ product yields, Atmos. Environ., 156, 125–134, https://doi.org/10.1016/j.atmosenv.2017.02.035, 2017c.

Wang, Y., Xi, S., Zhao, F., Huey, L. G., and Zhu, T.: Decreasing Production and Potential Urban Explosion of Nighttime Nitrate Radicals amid Emission Reduction Efforts, Environ. Sci. Technol., 57, 21306–21312, https://doi.org/10.1021/acs.est.3c09259, 2023b.

Wang, Z., Wang, W., Tham, Y. J., Li, Q., Wang, H., Wen, L., Wang, X., and Wang, T.: Fast heterogeneous N_2O_5 uptake and $ClNO_2$ production in power plant and industrial plumes observed in the nocturnal residual layer over the North China Plain, Atmos. Chem. Phys., 17, 12361–12378, https://doi.org/10.5194/acp-17-12361-2017, 2017d.

Wayne, R. P., Barnes, I., Biggs, P., Burrows, J. P., Canosa-Mas, C. E., Hjorth, J., Le Bras, G., Moortgat, G. K., Perner, D., Poulet, G., Restelli, G., and Sidebottom, H.: The nitrate radical: Physics, chemistry, and the atmosphere, Atmos. Environ. Part Gen. Top., 25, 1–203, https://doi.org/10.1016/0960-1686(91)90192-A, 1991.

Xia, M., Peng, X., Wang, W., Yu, C., Wang, Z., Tham, Y. J., Chen, J., Chen, H., Mu, Y., Zhang, C., Liu, P., Xue, L., Wang, X., Gao, J., Li, H., and Wang, T.: Winter $ClNO_2$ formation in the region of fresh anthropogenic emissions: seasonal variability and insights into daytime peaks in northern China, Atmos. Chem. Phys., 21, 15985–16000, https://doi.org/10.5194/acp-21-15985-2021, 2021.

Yan, C., Yee Jun, T., Nie, W., Xia, M., Wang, H., Guo, Y., Ma, W., Zhan, J., Li, Y., Deng, C., Li, Y., Zheng, F., Chen, X., Li, Q., Zhang, G., Mahajan, A., Cuevas, C. A., Huang, D., and Kulmala, M.: Increasing contribution of nighttime nitrogen chemistry to wintertime haze formation in Beijing observed during COVID-19 lockdowns, Nat. Geosci., 16, https://doi.org/10.1038/s41561-023-01285-1, 2023.

Yao, Y., Wang, S., Wei, N., Ye, C., Zhang, C., Gu, X., Zhao, W., and Zhang, W.: Analysis of surface ozone sources in Beijing during the 2022 Beijing Winter Olympic Games based on total peroxyl radical measurement, Acta Sci. Circumst., 43, 290–297, https://doi.org/10.13671/j.hjkxxb.2023.0070, 2023.

Yu, C., Wang, Z., Xia, M., Fu, X., Wang, W., Tham, Y. J., Chen, T., Zheng, P., Li, H., Shan, Y., Wang, X., Xue, L., Zhou, Y., Yue, D., Ou, Y., Gao, J., Lu, K., Brown, S. S., Zhang, Y., and Wang, T.: Heterogeneous N_2O_5 reactions on atmospheric aerosols at four Chinese sites: improving model representation of uptake parameters, Atmos. Chem. Phys., 20, 4367–4378, https://doi.org/10.5194/acp-20-4367-2020, 2020.

Yuan, Z., Lau, A. K. H., Shao, M., Louie, P. K. K., Liu, S. C., and Zhu, T.: Source analysis of volatile organic compounds by positive matrix factorization in urban and rural environments in Beijing, J. Geophys. Res. Atmos., 114, https://doi.org/10.1029/2008JD011190, 2009.

https://doi.org/10.5194/egusphere-2025-2210
Preprint. Discussion started: 17 June 2025

597 Yun, H., Wang, W., Wang, T., Xia, M., Yu, C., Wang, Z., Poon, S. C. N., Yue, D., and Zhou, Y.: Nitrate formation
598 from heterogeneous uptake of dinitrogen pentoxide during a severe winter haze in southern China, Atmos.
599 Chem. Phys., 18, 17515–17527, https://doi.org/10.5194/acp-18-17515-2018, 2018.
600 Zhang, H., Wang, S., and Hao, J.: Air pollution and control action in Beijing, J. Clean. Prod., 112, 1519–1527,
601 https://doi.org/10.1016/j.jclepro.2015.04.092, 2016.
602 Zhang, T., Zuo, P., Ma, J., Ye, C., Lin, W., and Zhu, T.: Characterization and Application of an Online
603 Measurement System for NO_3 and N_2O_5 Based on Cavity Ring-Down Spectroscopy, Acta Sci. Nat. Univ.
604 Pekin., 60, 563–574, https://doi.org/10.13209/j.0479-8023.2024.030, 2024.
605 Zhang, T., Ma, J., Liu, T., Lin, W., Zuo, P., and Ye, C.: A dynamic generation system for NO_3 and N_2O_5 standard
606 gases, Environ. Chem., 45, 1–7, https://doi.org/10.7524/j.issn.0254-6108.2024091302, 2026.
607 Zhang, T., Zuo, P., Chen, Y., Liu, T., Zeng, L., Lin, W., and Ye, C.: Measurement report: Variations and
608 environmental impacts of atmospheric N_2O_5 concentrations in urban Beijing during the 2022 Winter
609 Olympics, Zenodo [data set], https://doi.org/10.5281/zenodo.15381990, 2025.
610 Zhang, X., Tong, S., Jia, C., Zhang, W., Li, J., Wang, W., Sun, Y., Wang, X., Wang, L., Ji, D., Wang, L., Zhao,
611 P., Tang, G., Xin, J., Li, A., and Ge, M.: The Levels and Sources of Nitrous Acid (HONO) in Winter of
612 Beijing and Sanmenxia, J. Geophys. Res. Atmos., 127, e2021JD036278,
613 https://doi.org/10.1029/2021JD036278, 2022.
614 Zhou, J., Zhao, W., Zhang, Y., Fang, B., Cheng, F., Xu, X., Ni, S., Zhang, W., Ye, C., Chen, W., and Venables,
615 D. S.: Amplitude-Modulated Cavity-Enhanced Absorption Spectroscopy with Phase-Sensitive Detection:
616 A New Approach Applied to the Fast and Sensitive Detection of NO_2, Anal. Chem., 94, 3368–3375,
617 https://doi.org/10.1021/acs.analchem.1c05484, 2022.
618 Zhou, W., Zhao, J., Ouyang, B., Mehra, A., Xu, W., Wang, Y., Bannan, T. J., Worrall, S. D., Priestley, M., Bacak,
619 A., Chen, Q., Xie, C., Wang, Q., Wang, J., Du, W., Zhang, Y., Ge, X., Ye, P., Lee, J. D., Fu, P., Wang, Z.,
620 Worsnop, D., Jones, R., Percival, C. J., Coe, H., and Sun, Y.: Production of N_2O_5 and $ClNO_2$ in summer in
621 urban Beijing, China, Atmos. Chem. Phys., 18, 11581–11597, https://doi.org/10.5194/acp-18-11581-2018,
622 2018.
623 Zhu, T., Tang, M., Gao, M., Bi, X., Cao, J., Che, H., Chen, J., Ding, A., Fu, P., Gao, J., Gao, Y., Ge, M., Ge, X.,
624 Han, Z., He, H., Huang, R.-J., Huang, X., Liao, H., Liu, C., Liu, H., Liu, J., Liu, S. C., Lu, K., Ma, Q., Nie,
625 W., Shao, M., Song, Y., Sun, Y., Tang, X., Wang, T., Wang, T., Wang, W., Wang, X., Wang, Z., Yin, Y.,
626 Zhang, Q., Zhang, W., Zhang, Y., Zhang, Y., Zhao, Y., Zheng, M., Zhu, B., and Zhu, J.: Recent Progress in
627 Atmospheric Chemistry Research in China: Establishing a Theoretical Framework for the “Air Pollution
628 Complex”※, Adv. Atmos. Sci., 1339–1361, 2023.